IEEE Antennas & Propagation Magazine

Volume 45, No. 6, December 2003 www.ieeeaps.org (ISSN 1045-9243)

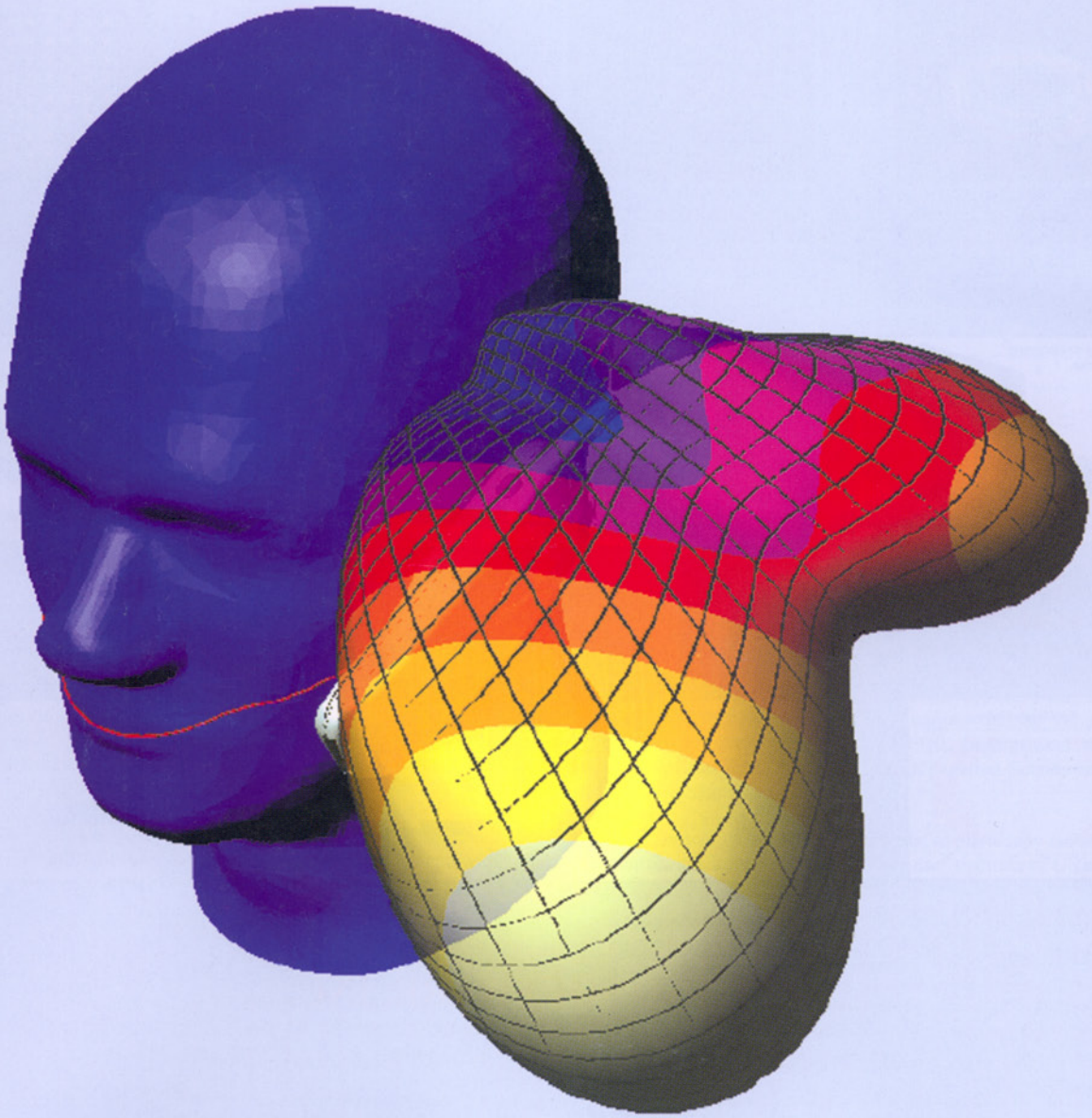

Suitability of FDTD-Based TCAD Tools for RF Design of Mobile Phones

Nicolas Chavannes[1], Roger Tay[2], Neviana Nikoloski[3], and Niels Kuster[3]

[1]Integrated Systems Laboratory, Swiss Federal Institute of Technology (ETH)
ETZ, Gloriastrasse 35, CH-8092 Zurich, Switzerland
Tel: +41-1-245-9700; Fax: +41-1-245-9779; E-mail: chavanne@iis.ee.ethz.ch

[2]Motorola Electronics Private Limited
Singapore Design Center, Motorola Innovation Center,
12 Ang Mo Kio Street 64, Ang Mo Kio Industrial Park 3, Singapore 569088
Tel: +65-6-482-3841; E-mail: roger.tay@motorola.com

[3]Foundation for Research on Information Technologies in Society (IT'IS)
Zeughausstrasse 43, 8004 Zurich, Switzerland
Tel: +41-1-245-9696; Fax: +41-1-245-9699; E-mail: neviana@itis.ethz.ch; kuster@itis.ethz.ch

Abstract

This paper discusses the general suitability and possible limitations of an enhanced Finite-Difference Time-Domain (FDTD) simulation environment for straightforward and efficient RF design of complex transmitters. The study was conducted using a current commercially available multi-band mobile phone. Simulations were conducted in free space and with various dielectric loads, whereby different parameters were evaluated such as impedance, efficiency, far-field as well as near-field distributions of E and H fields, and the specific absorption rate (SAR). The results were compared to measurements. In addition, mechanical-design issues that showed a significant influence on the electromagnetic (EM) field behavior could be predicted by simulations and were experimentally reproduced. The accurate prediction of all essential performance parameters obtained by straightforward simulations suggests that appropriately enhanced software packages are suitable for device design in industrial research and development environments with few limitations, provided flexible graphical user interfaces (GUIs) and graded meshes combined with local grid-refinement schemes are available.

Keywords: FDTD methods; numerical analysis; simulation software; software tools; computer aided analysis; computer aided engineering; design automation; mobile communication; mobile antennas; multifrequency antennas; antenna measurements; dosimetry; research and development; land mobile radio cellular equipment

1. Introduction

The last two decades have shown tremendous growth within the mobile telecommunications equipment (MTE) sector. Furthermore, consumers have put high demands on excellent product quality combined with low pricing. Due to increasing competition and rapid market expansion, the life cycles of the products themselves and, hence, device-development cycles are getting shorter. In addition, new requirements have recently been introduced, such as mandatory safety guidelines defined by the regulatory agencies [1, 2, 3, 4]. The market might demand even more efficient devices, due to increased public concern about possible adverse health effects of radio-frequency (RF) exposure.

These new challenges for RF engineers clearly call for new analysis and optimization tools. Technical computer-aided design (TCAD) is the answer, provided that these tools can be applied to real-world designs in a straightforward user-friendly manner. The needs are obvious:

- The ability to import and easily manipulate/modify standard mechanical computer-aided design (CAD) data formats;
- Easy and accurate composition of different complex objects (consisting of hundreds of different sub-volumes), i.e., different positions of a mobile phone at the human head;
- Resolutions of a few μm within relatively large environments (of the order of 1 m);
- Handling of perfectly electrically conducting (PEC) structures embedded in dielectric and lossy material/objects, as well as provisions for lumped elements;
- Computation of all relevant parameters, such as feed-point impedance, radiation pattern, efficiency, heat distribution, etc.;
- Efficient model generation, short result return time, uncertainty assessment, and result visualization that is directly comparable to measured results;

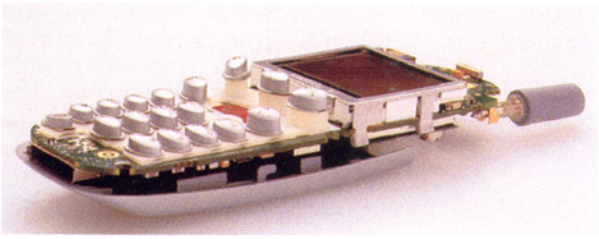

Figure 1a. The physical model of the Motorola T250 phone.

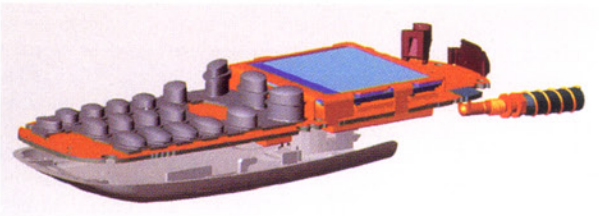

Figure 1b. The numerical equivalent of the physical model for the T250 phone used for the FDTD simulations.

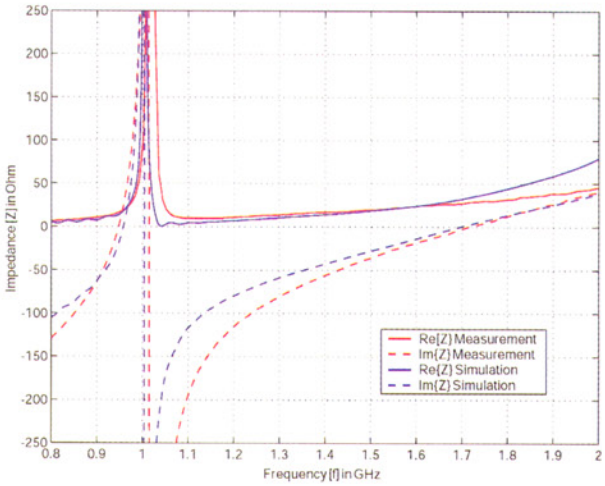

Figure 6. A comparison of the measured and simulated impedance for the multi-band antenna in the frequency range from 800 MHz to 2 GHz.

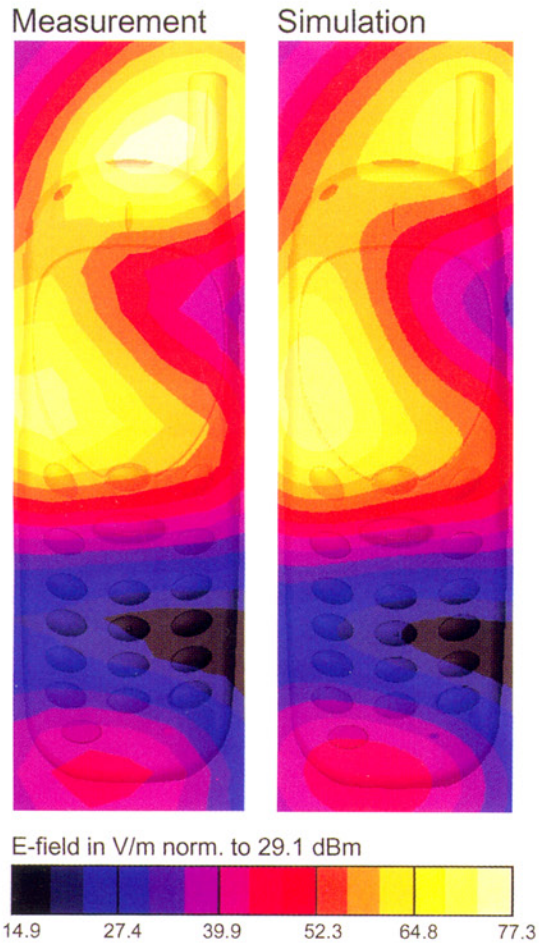

Figure 7a. A comparison of the simulation and measurement for the electric field (DCS1800), shown in a plane located 10 mm above the phone (from the highest point). All fields were normalized to 29.1 dBm.

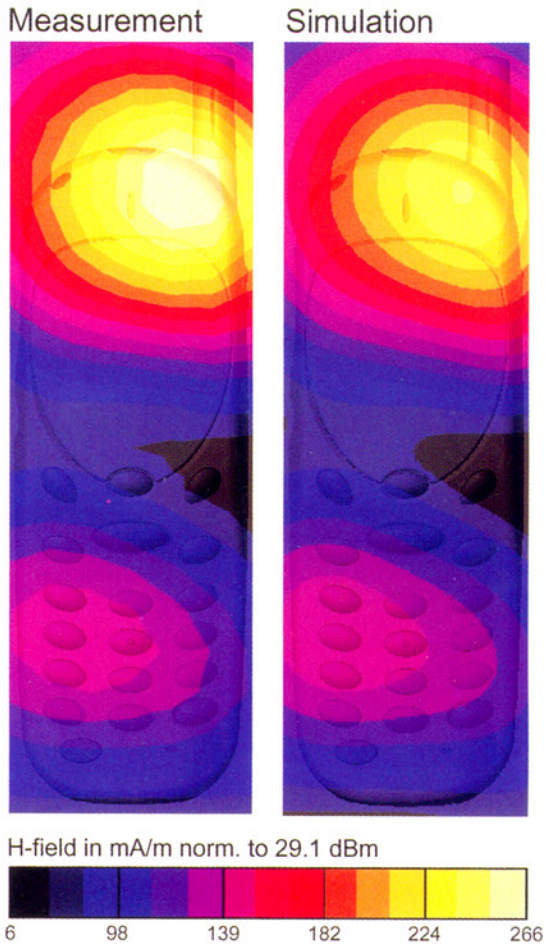

Figure 7b. A comparison of the simulation and measurement for the magnetic field (DCS1800), shown in a plane located 10 mm above the phone (from the highest point). All fields were normalized to 29.1 dBm.

- Semi-automated optimization by genetic algorithm (GA).

Various numerical methods have been developed and applied for the analysis of antennas, e.g., the Method of Moments (MoM), the General Multipole Technique (GMT), the Finite-Element Method (FEM), and the FDTD method. Although some of these algorithms are well suited for the design of basic or very specific antennas, their general application to structures embedded in largely non-homogeneous and lossy environments is very difficult or impossible. The Finite-Difference Time-Domain (FDTD) technique has gained growing interest because of its robustness, suitability for handling complex problems composed of any number of sub-volumes, and general independence of material composition. The exponential growth of computer performance, as well as various enhancements of the technique [5, 6, 7] originally presented by Yee [8], has made FDTD the most popular and most widely applied technique [9, 10, 11]. However, some limitations of FDTD have included the following:

1. Real-world problems often consist of small structures embedded in a relatively large computational space. An example is unintended capacitive coupling among the electromechanical components, display, battery, and RF shields inside a mobile phone that is operated in close proximity to a human head. These structures may have spatial dimensions of only a few μm, while the computational space may reach one meter or more. Only a combination of graded meshes with sub-grids can enable FDTD to handle such structures. Previous studies required strong simplifications, such as rectangular metal boxes equipped with monopole- or dipole-like structures. Pioneering efforts in helix modeling were performed primarily by "stair-cased" wire approximations [10, 12, 13, 14].

2. The restriction to a rectangular grid can result in unacceptable uncertainties, due to the stair-stepped approximation of curved structures, or structures non-conformally aligned with the grid [15, 16]. This can be particularly true for complex mobile-telecommunications equipment-head configurations [17]. Whereas certain studies have approximated the entire internal structure of CAD-derived mobile phones by single perfectly electrically conducting blocks [18, 19], the inclusion of specific interior parts was modeled (e.g., in [20]) by application of rather coarse grid resolutions of about 1 mm. The investigations presented in this paper point out the importance of appropriate modeling, including significant internal mobile-telecommunications equipment structures modeled with a highly refined FDTD mesh.

3. Although generation of the FDTD grid is trivial compared to grid-mesh generation in other methods (e.g., FEM), an optimized grid can significantly reduce the computation time and improve the accuracy of the results. Some software packages operate on a predefined grid; others do not allow the handling of objects composed of hundreds of polyhedra, or do not support the use of grid optimization [21]. The use of enhanced modeling schemes is particularly recommended [22] for the analysis of finely detailed structures, such as the antennas used in mobile-telecommunications equipment, which are embedded within extended spatial environments. High efficiency can then be achieved by the combination of optimized graded-mesh [23] and local-refinement schemes.

The objective of this study was to evaluate whether FDTD-based tools can be utilized for supporting RF engineers in the design of mobile phones. This clearly demands simulation of not only the outer shape of the device, but all embedded electromechanical components that are RF relevant, as shown in Figure 1. Resolutions down to 100 μm or less are required. The quality of the simulations was validated with measurement results utilizing the Dosimetric Assessment System (DASY) V4 near-field scanners.

2. Mobile Phone

The phone selected for this study was a current commercially available tri-band phone (GSM, DCS, PCS), the Motorola, Inc., T250. Two samples of the phone were purchased in Zurich for the purpose of this study. The first model was used only for measurements; the second was disassembled and examined. The product was designed at Motorola using the *ProEngineer* CAD platform. The CAD dataset was consequently exported in stereolithography (STL) format for the purpose of modification and modeling within the Simulation Platform for Electromagnetic Compatibility, Antenna Design and Dosimetry (*SEMCAD*). The results for only the two main bands are reported in this paper, namely GSM and DCS.

3. Numerical Method

The FDTD-based platform *SEMCAD* [24] was used for all simulations performed. *SEMCAD* is the internal simulation platform applied within our research group for the performance of electromagnetic computations. It is continuously improved and extended by a Swiss Consortium composed of the Integrated Systems Laboratory of ETHZ, IT'IS, SPEAG, and Integrated Systems Engineering (ISE) AG. The solid-modeling environment is based on the *ACIS*® modeling toolkit, and allows the user-defined generation of three-dimensional objects, as well as the importation of entire CAD datasets. The FDTD kernel provides three-dimensional full-wave simulation, and operates on a non-homogeneous rectilinear grid. This allows the grid-independent positioning, tilting, and moving of objects before performing the material assignment.

The kernel was extended by a novel sub-gridding scheme proposed in [25], combined with semi-automated grid generation. Since the mobile-phone CAD dataset consisted of very detailed parts – such as printed-circuit-board (PCB) layers and a helical antenna with a minimum spatial extent of 100 μm – a common graded-mesh approach would have led to a large number of Yee cells for the computational space, particularly when placed beside a head model. The use of such FDTD local-refinement modeling techniques was therefore necessary in order to reduce the computational requirements to a tolerable level. The combined platforms *SEMCAD* and DASY4 (see Section 4) allowed a direct comparison of numerical and experimental data within the same post-processing environment.

4. Measurement Technique

The measurements were conducted with the near-field scanning system DASY4 (Schmid & Partner Engineering AG, Switzerland), which is the fourth generation of the system described in [26], as shown in Figure 2. The scanner was equipped with the probes providing the required isotropy, sensitivity, and spatial resolution (see Table 1). The phantom used was the Twin SAM

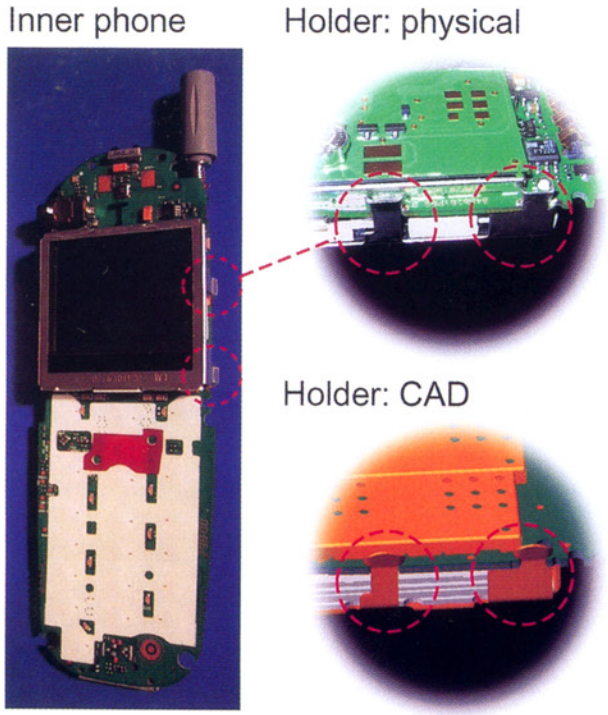

Figure 8. The physical model and CAD representation of the metallic holder for the LCD structure.

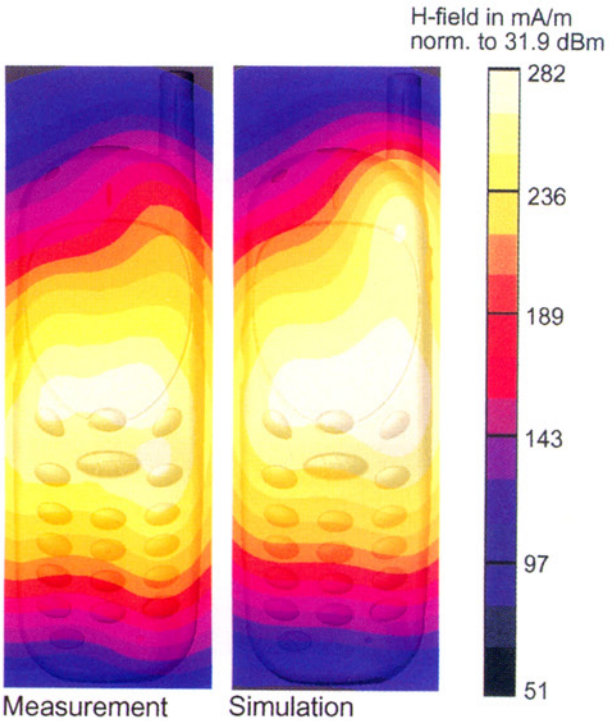

Figure 9a. The measured and simulated results for the floating LCD holder, in a plane located 5 mm above the highest point on the phone. All fields were normalized to 31.9 dBm.

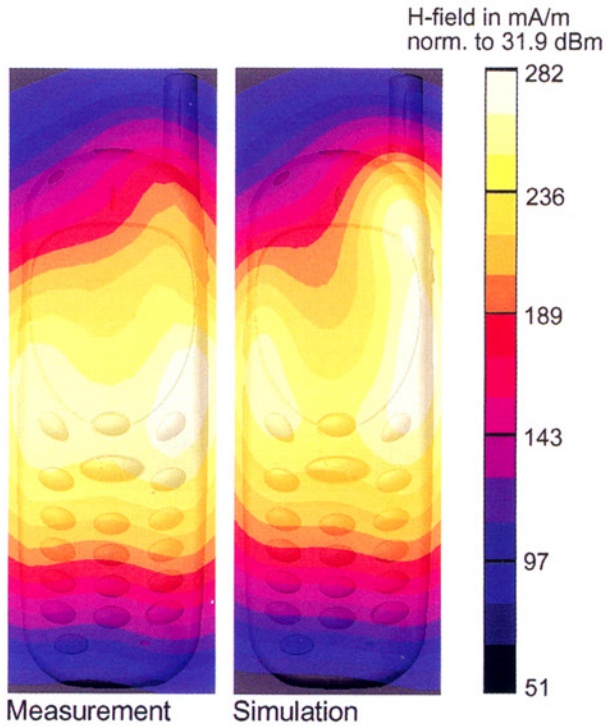

Figure 9b. The measured and simulated results for the connected LCD holder, in a plane located 5 mm above the highest point on the phone. All fields were normalized to 31.9 dBm.

Figure 2. The DASY4 automated dosimetric assessment system, shown making a free-space measurement of the mobile phone.

Table 1. The DASY4 probes employed for the experimental evaluation. The dynamic range was equal to or larger than 0.1 - 3 GHz, and the linearity was better than ± 0.2 dB for all probes.

Probe Type	Diameter [mm]	Dynamic Range	Dev. of Axial Isotropy [dB]	Dev. of Spherical Isotropy [dB]
ET3DV6 1374	6.8	2μW-0.1W/g	< ±0.05	< ±0.20
ET3DV2 4004	3.9	2-1000 V/m	< ±0.05	< ±0.30
ET3DV6 6060	5.0	0.01-2 A/m	< ±0.12	< ±0.20

[27], which has recently been standardized for antenna-performance characterization by various organizations. The probes and the system were calibrated according to [28, 29].

5. FDTD Modeling

5.1 Implementation of Phone

The first step was to import the CAD dataset, which was provided in STL format. In order to distinguish the individual pieces and to enable an assignment of the different material properties, each sub-file was imported separately. The dataset consisted mainly of electromechanical parts, such as the following:

- triple-band antenna
- PCB
- shields
- LCD and its holder
- lenses, and housing parts
- keypad and buttons
- battery and battery contact
- connectors

The phone was oriented with the PCB conformally aligned with an FDTD primary grid plane, in order to reduce stair-casing effects for the largely extended PEC structure. Whereas the basic dielectric parts such as the housing and buttons were maintained as imported into the FDTD platform, special attention was paid to particular pieces that significantly influenced the EM-field behavior. The mechanical PCB part originally consisted of just one single PEC block; this had to be changed, in order to represent internal losses. Two dielectric layers were consequently embedded into three PEC ground layers. The grounds were connected to each other by 50 vias, which were uniformly distributed over the entire PCB area. Figure 3 illustrates a detail of the PCB structure. The PCB ground and dielectric layers were modeled at thicknesses of 110 μm and 450 μm, respectively. A representation of the PCB structure, incorporating additional components and details such as conductor paths, cabling, integrated circuits (ICs), etc., has not been developed.

All metallic parts were modeled as perfect electric conductors, which was acceptable at the observed frequencies (902 MHz, 1747 MHz). The dielectric components were represented within the FDTD simulation using the material parameters summarized in Table 2. These parameters corresponded to measured data provided by the manufacturers of the different electromechanical parts.

5.2 Source Representation

In order to achieve proper excitation of the mobile-phone structure, a source region was modeled that corresponded to the excitation of the physical phone. Figure 4 depicts the detailed setup in the CAD environment. To achieve an electric separation from the antenna to the PCB, a small region of the upper PCB

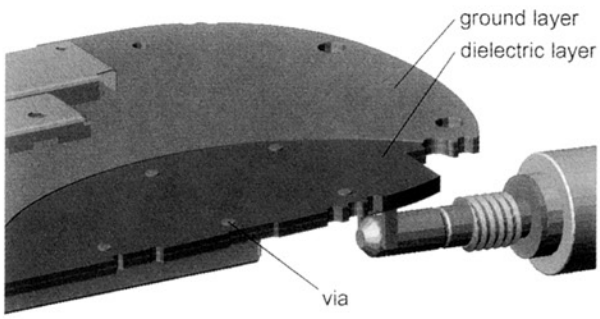

Figure 3. The numerical PCB structure, consisting of two dielectric and three PEC layers, as well as the interconnecting vias.

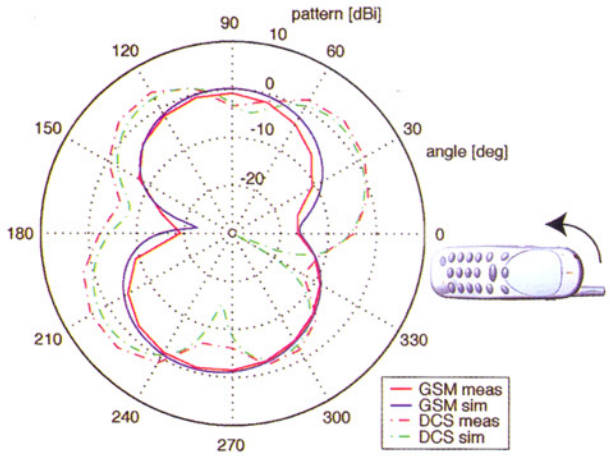

Figure 10a. The measured and simulated two-dimensional radiation pattern (*xy* plane, horizontal polarization) for the T250 phone in free space for the GSM900 and DCS1800 frequency bands.

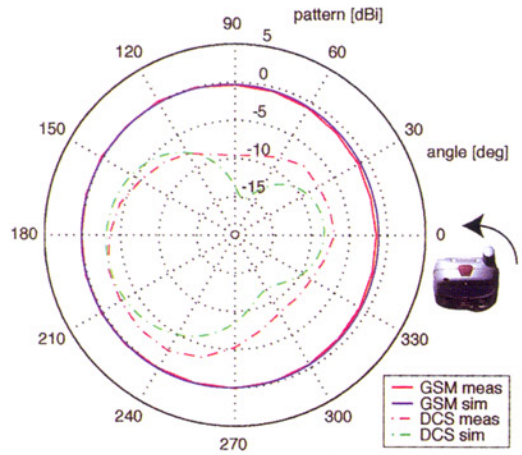

Figure 10b. The measured and simulated two-dimensional radiation pattern (*xz* plane, vertical polarization) for the T250 phone in free space for the GSM900 and DCS1800 frequency bands.

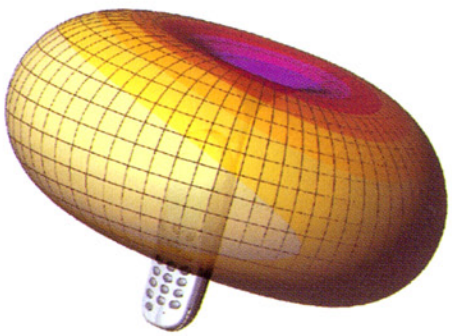

Figure 11a. The three-dimensional radiation pattern of the T250 mobile phone in free space, operating in the GSM900 band.

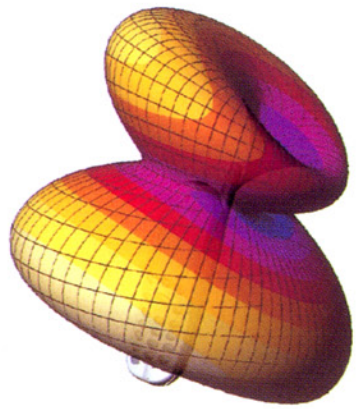

Figure 11b. The three-dimensional radiation pattern of the T250 mobile phone in free space, operating in the DCS1800 band.

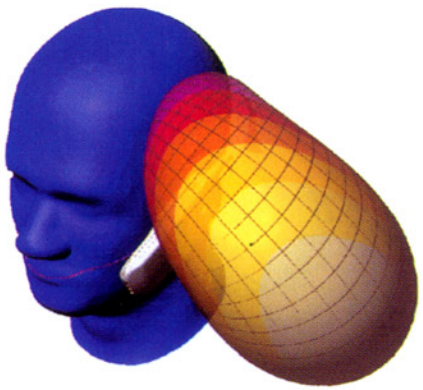

Figure 11c. The three-dimensional radiation pattern of the T250 mobile phone next to the SAM phantom, operating in the GSM900 band.

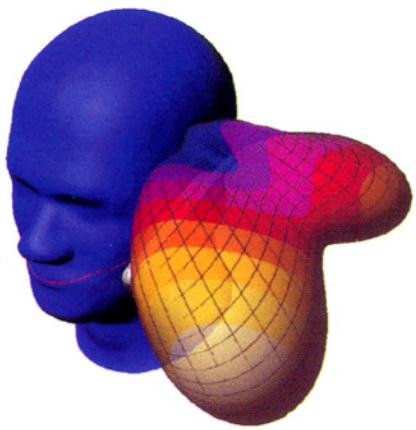

Figure 11d. The three-dimensional radiation pattern of the T250 mobile phone next to the SAM phantom, operating in the DCS1800 band.

Table 2. The main dielectric parts of the mechanical CAD data set and the corresponding material parameters.

Part	ε_r	$\sigma\left[\frac{S}{m}\right]$
Antenna bushing	2.5	3e-3
Antenna cover	2.5	3e-3
PCB dielectric	4.5	7e-2
LCD glass	4.5	1e-2
LCD dielectric	3	1e-2
IrDa dielectric	3.5	2e-2
Housing	3.5	2e-2
Keypad/buttons	3.5	2e-2

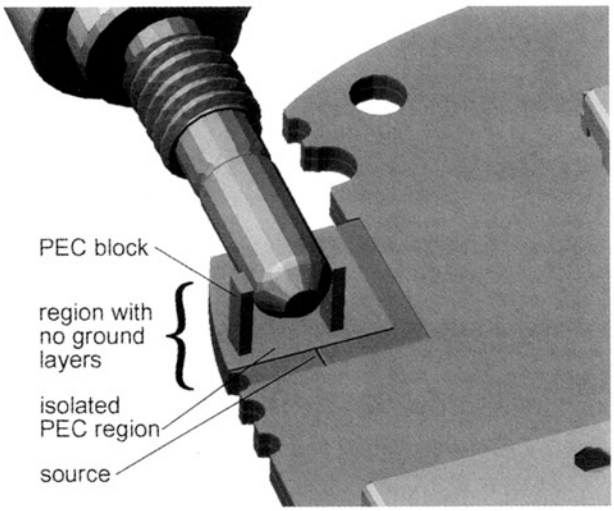

Figure 4. The excitation of the antenna-PCB structure in the modified source region.

ground layer was isolated from its main part by introducing an air gap of 1 mm thickness. The discrete source was consequently placed between the resulting PEC island-like plate and the remaining ground layer (the indicated line in Figure 4). The plate itself was connected to the antenna stem using two PEC blocks, similarly to the connection in the physical mode. To reduce capacitive coupling from the island-like PEC plate to the middle and lower ground layers, the grounding was removed and replaced with dielectric material within the specified region.

The design of the physical phone did not allow direct determine of information at the feed-point. Therefore, the comparison between simulation and measurement was not performed based on the feed-point impedance. Instead, an antenna input power that was assessed indirectly by matching simulated near-field distributions with measured distributions was used (Section 4). Consequently, a single discrete source element was applied for the excitation of the mobile phone. In order to reach steady state within the simulation more quickly, the source itself was modeled by a resistive ($50\,\Omega$) voltage source as proposed in [30], allowing energy in the system to be diminished. The $50\,\Omega$ resistance did not affect the feed-point impedance of the simulated phone. Moreover, any influence of the voltage source on the assessed near- and far-field data was compensated for via normalization to the radiated power.

Due to the fairly broad extension of the source gap (1 mm), it was discretized using three primary Yee-grid edges, i.e., the source was applied to one edge, whereas the remaining two edges were defined as PECs. Two signal forms were applied as excitation:

1. To assess EM-field information at a specific frequency, a harmonic sinusoidal excitation, with a two-period rising signal, was used. The system reached steady state after 13 periods.

2. To assess broadband frequency-domain information, a Gaussian sine pulse, with a bandwidth $B = 1.5\,\text{GHz}$, was applied. For this case, the simulation reached steady state after 8 ns.

Most of the results shown in Section 6 are related to the main GSM frequency at transmitting bands with center frequencies of 902 MHz and 1747 MHz, specified as the GSM900 and DCS1800 bands, respectively.

5.3 Grid Generation/ Simulation Parameters

The simulation platform *SEMCAD* incorporates semi-automated non-homogeneous grid generation, which automatically adapts the mesh to a specific setup. In addition, the mesh can be manually configured to match particular user-defined requirements. In order to reduce memory and runtime requirements, the local refinement scheme (Section 3) was applied to resolve certain regions of the phone model with high resolution. The most crucial parts with respect to grid resolution were the antennas, including the helical-wire and monopole (0.65 mm wire diameter), as well as the PCB with its thin PEC ground layers (110 μm thickness).

Since the helical antenna is highly non-conformally aligned to the FDTD grid, it had to be resolved by multiple cells in the wire diameter, in order to accurately represent its field distribution. A spatial resolution of $0.2 \times 0.2 \times 0.1\ \text{mm}^3$ in the x, y, and z directions was chosen within the sub-grid (a 1:2 refinement factor) surrounding the antenna, consisting of about 500×10^3 mesh cells in total. Figure 5 depicts this configuration, with the combined graded mesh and sub-grid.

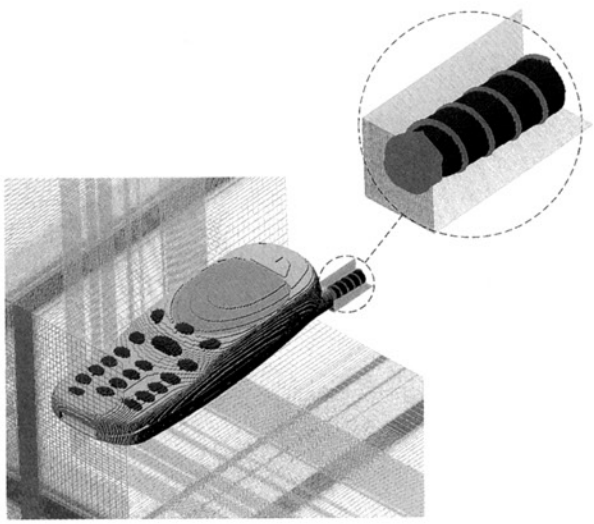

Figure 5. The application of the FDTD grid: a combination of a graded mesh and a sub-grid (helical antenna).

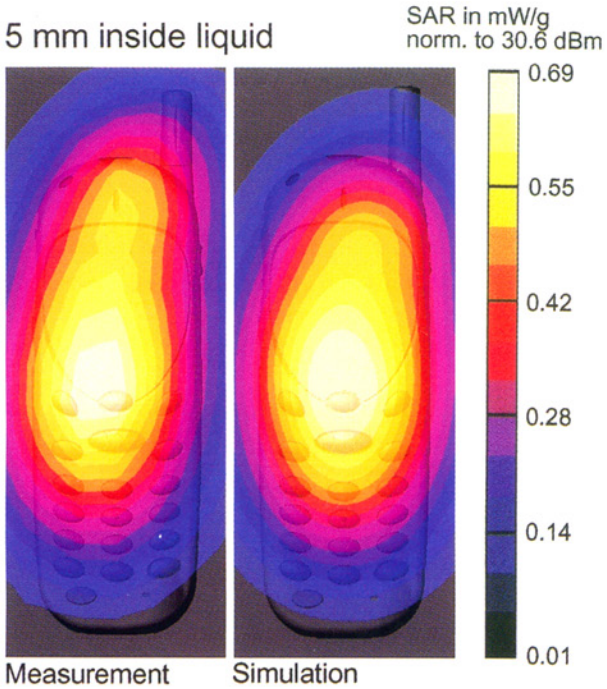

Figure 12a. A comparison of the simulated and measured results for the SAR distribution within the flat phantom at 902 MHz. The observation plane was located 5 mm from the inner phantom surface. All fields were normalized to 30.6 dBm.

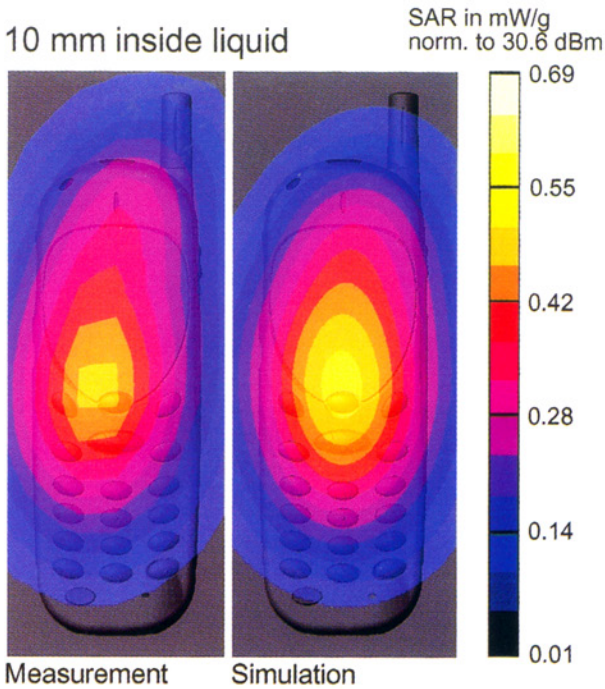

Figure 12b. A comparison of the simulated and measured results for the SAR distribution within the flat phantom at 902 MHz. The observation plane was located 10 mm from the inner phantom surface. All fields were normalized to 30.6 dBm.

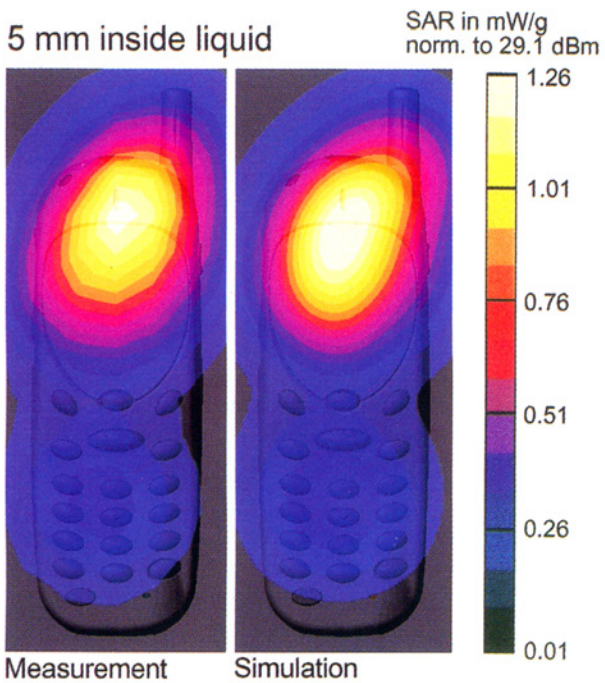

Figure 13a. A comparison of the simulated and measured results for the SAR distribution within the flat phantom at 1747 MHz. The observation plane was located 5 mm from the inner phantom surface. All fields were normalized to 29.1 dBm.

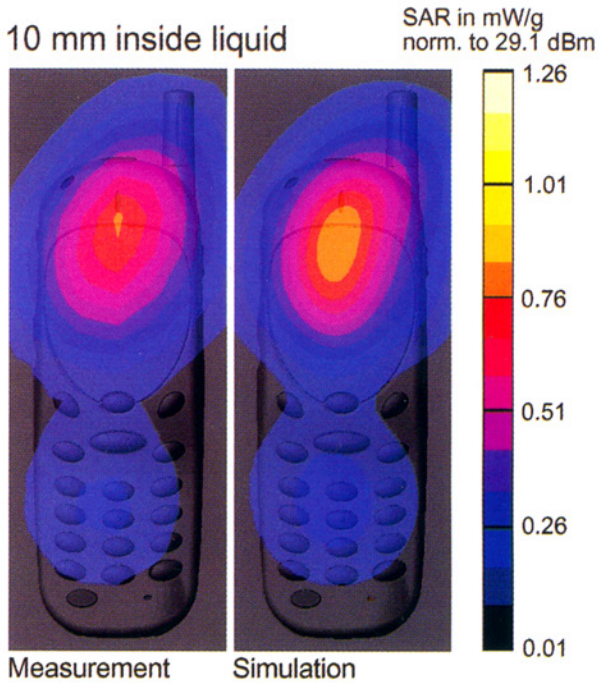

Figure 13b. A comparison of the simulated and measured results for the SAR distribution within the flat phantom at 1747 MHz. The observation plane was located 10 mm from the inner phantom surface. All fields were normalized to 29.1 dBm.

The PCB structure was resolved with a slightly higher resolution of 200 μm, which properly resolved all dielectric and PEC ground layers. Furthermore, for configurations including head models, the sub-grid used to represent the PCB part was slightly extended in the z direction, enclosing the most significant absorbing parts of the head. Its x, y, and z axis resolution of $0.4 \times 0.4 \times 0.2$ mm^3 resulted in a total of about 5.5 million cells.

Within the free-space simulation, the computational domain was extended about $0.75\,\lambda$ (at $f = 902$ MHz) in each spatial direction (the distance to the phone boundaries). In order to avoid the introduction of additional errors caused by stair-casing, the PCB was left conformally oriented to the FDTD grid. The standard positions for compliance testing were achieved by rotation of the lossy dielectric head models. For the outer grid in the free-space simulation, a non-homogenous mesh using an increasing mesh step of from 0.2 mm up to 7 mm (a grading ratio of 1.5) was chosen, which led to four million cells. The simulations including head models consisted of the same minimum and maximum mesh steps, with the human-ear region being modeled with a grid resolution of $0.4 \times 0.4 \times 0.2$ mm^3, leading to a total of about six million cells.

All simulations were bounded by a perfectly matched layer (PML) [31] absorbing boundary condition (ABC), with a layer thickness of eight cells.

Using *SEMCAD*, the total time needed to import and modify the phone model (PCB structure, source region) as well as its positioning beside a numerical head phantom and the appropriate FDTD grid generation was about one day. Further modifications (Section 6.3) were achieved within a few additional hours.

6. Results and Validation

The physical device was put into operation using a Rhode & Schwarz Radio Communication Tester CTS55 for the experimental evaluations. The middle traffic channels were utilized for both the GSM900 and DCS1800 systems, i.e., they were operated at $f = 902.4$ MHz and $f = 1747.4$ MHz, respectively. The power level was set to its maximum for both GSM and DCS, i.e., Power Control Level 5 (33 dBm) and Power Control Level 0 (30 dBm), respectively. Communication between the tester and the device was established by an active network link.

The phone design did not enable direct measurement of the antenna input power with sufficient precision. For the purpose of this comparison, the antenna input power was determined indirectly, by matching the simulated H-field distributions with measured distributions from the DASY system. In order to achieve minimum uncertainty, a global least-squares fit was conducted on the H-field distributions of free space at different distances and inside the flat phantom. The inclusion of the information regarding the reactive near field provided a more reliable determination of the input power at the feed point than conductive power measurements, or measurement of the radiated power in the far field.

The values obtained for the slot-averaged antenna input power to which all reported simulation results were normalized were 30.6 dBm (GSM900) and 29.1 dBm (DCS1800).

6.1 Validation of Antenna Model

Prior to the simulation of the complete phone model, the multi-band antenna was examined by measurement and simulation as a monopole over a finite ground plane, in order to ensure proper representation of the antenna structure. In order to reduce the computational requirements, the CAD antenna structure was modeled by application of a 1:8 sub-gridded region around it (125 μm^3 resolution), consisting of two million cells. A non-homogeneous mesh using mesh cells from 1 mm to 9 mm was used (a grading ratio of 1.4) within the main grid, which led to a total of one million cells. The computation domain would have consisted of 15 million cells without making use of a local refinement scheme.

Figure 6 compares the measured and simulated impedances in the frequency range from 800 MHz to 2 GHz. Regarding the complexity of the multi-band antenna model, the general agreement of both real and imaginary parts is good. In particular, the resonance frequencies matched very well, leading to 948 MHz and 960 MHz (lower resonance) and to 1.695 GHz and 1.712 GHz (higher resonance) for the measured and simulated impedances, respectively.

6.2 Free-Space EM Field Distribution

Figure 7 depicts the measured and simulated E- and H-field distributions at the DCS1800 frequency. The fields were recorded in a plane located 10 mm above the highest point of the phone (the display), whereby the PCB was horizontally aligned in space. In order to reduce possible influence from nearby dielectrics, the phone was placed on Styrofoam, as shown in Figure 2.

The comparison of the simulated and the measured distributions shows slight deviations in the region of the maximum, mainly close to the antenna. However, the general agreement for both characteristic E- and H-field patterns is very good.

6.3 Design Capabilities: Effect of the LCD Holder Connection

In order to assess the capabilities of the proposed simulation techniques with respect to design purposes, special attention was given to electromechanical parts that appeared to have a significant impact on the EM-field behavior. Furthermore, the influence of the FDTD grid resolution on the current distribution was examined. Major differences between simulation and measurements were initially obtained, particularly in the region of the liquid-crystal display (LCD), which was mechanically fixed to the PCB via a holder, and electrically connected via four clamps (Figure 8). This effect occurred mainly at $f = 902$ MHz, since the current distribution on the phone at this particular frequency was localized to the LCD region. A closer investigation of the physical holder revealed that the clamps actually did not create a proper RF short circuit to the PCB ground. Therefore, both models (CAD and physical) were modified in a manner so as to represent a *holder-connected* and a *holder-floating* situation. These modifications were realized on a

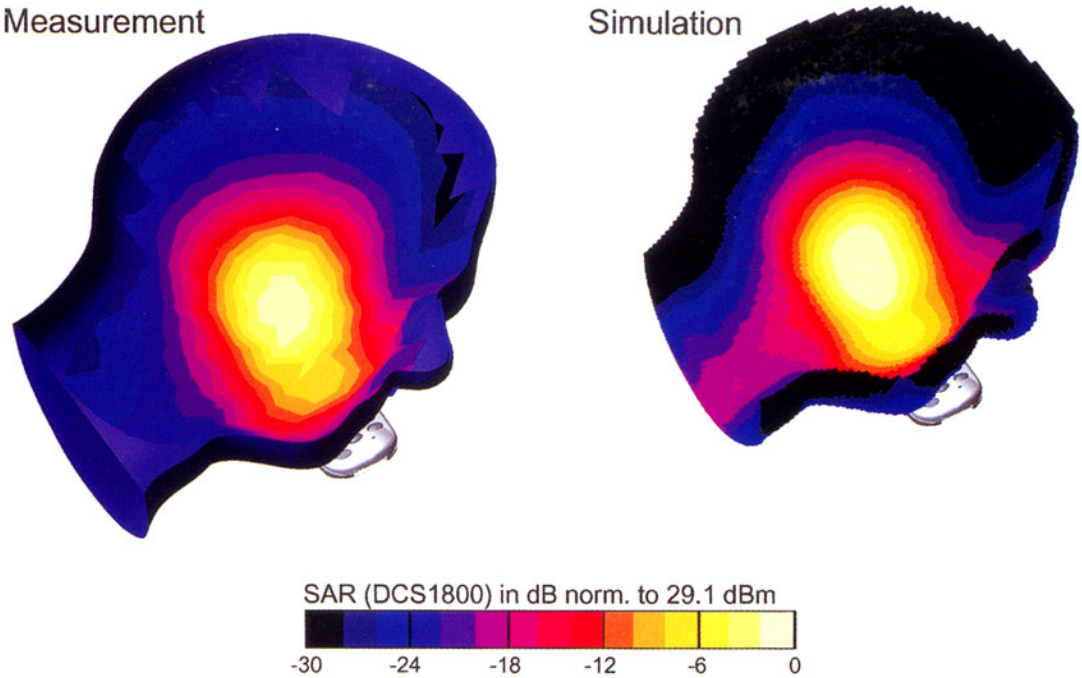

Figure 15. The measured and simulated SAR distributions within the SAM phantom (left side touch position, GSM1800).

Figure 16. The T250 phone model placed beside the high-resolution European female numerical head phantom (HR-EF-1).

third physical phone model, in order not to change the high-frequency behavior of the main device. All fields were normalized to an input power of 31.9 dBm, similarly to the procedure described in Section 6.2.

As shown in Figure 9, the LCD holder-connection-related EM-field distribution predicted by the FDTD simulation was reproduced within the measured data. It was observed that for a properly connected holder, the currents were capable of flowing on either side of the frame, whereas a floating holder led to a much higher concentration of the H field in the central region of the phone.

6.4 Free-Space Radiation Pattern

The measured and simulated radiation patterns of the T250 mobile phone, located in free space, are compared in Figure 10. In the FDTD simulation, the far-field pattern was determined using a near-to-far-zone transformation, as proposed in [32]. The experimental assessment of the radiation characteristics was performed in a rectangular anechoic chamber. Figure 10 shows the radiation pattern for horizontal and vertical polarization within the *x-y* and *x-z* planes in dBi for the GSM900 and the DCS1800 bands, respectively. Good agreement between measurement and simulation was obtained for both polarizations in the Cartesian planes observed. Due to the smaller number of data points recorded in the experimental assessment, the field minima were not determined properly, leading to deviations in these regions. The three-dimensional far-field patterns extracted from the simulation are depicted in Figure 11 for both frequency bands.

6.5 Performance at Flat Phantom

Since the phone is usually operated in the vicinity of the human body, it is essential that the simulations can appropriately predict the performance for these conditions. The first evaluation was conducted with the well-characterized shape of a flat phantom, which is the test configuration for body-mounted operation. The phone was therefore positioned with its PCB horizontally aligned, and its highest point touching the plastic shell of the Specific Anthropomorphic Mannequin (SAM) twin-phantom flat section [27]. The height of the liquid simulating brain tissue was 80 mm. The dielectric parameters for the liquid and shell that were used in the measurement and simulation at both GSM900 and DCS1800 frequencies are shown in Table 3. They are consistent with the values proposed in [33], which were derived from worst-case considerations.

Figures 12 and 13 depict the measured and simulated SAR distributions within the liquid at 902 MHz and 1747 MHz for two distances of 5 mm and 10 mm from the inner surface of the shell. Although the regions of maximum showed slight deviations between the experimental and numerical data, very good agreement was obtained in most of the area observed.

Table 4 summarizes the measured and simulated values for the peak SAR averaged over cubes of 1 g and 10 g mass at both frequencies, according to the procedure described in [34]. Comparisons of the two methods yielded excellent agreement for all values. The small deviations resulted from a possible cancellation of errors within the uncertainties of the simulation, and the tolerances of the measurement system.

Table 3. The material parameters for the SAM phantom.

Material	902 MHz		1747 MHz	
	ε_r	$\sigma\left[\frac{S}{m}\right]$	ε_r	$\sigma\left[\frac{S}{m}\right]$
Liquid	41.5	0.97	40.0	1.40
Shell	3.5	0	3.5	0

Table 4. The 1 g and 10 g averaged SAR values for the phone in the flat phantom configuration.

Type	SAR_M [W/kg]	SAR_S [W/kg]	Diff [%]
902 MHz_{1g}	0.71	0.74	+4.2
902 MHz_{10g}	0.48	0.49	+2.1
1747 MHz_{1g}	1.2	1.34	+11.7
1747 MHz_{10g}	0.72	0.75	+4.2

Table 5. The 1 g and 10 g averaged SAR values for the left application side *Touch* position for the SAM and human-head phantoms.

Type	SAR_M [W/kg]	SAR_S [W/kg]	SAR_H [W/kg]	Diff $[M-S]$ [%]
902 MHz_{1g}	0.86	0.91	0.77	+5.8
902 MHz_{10g}	0.58	0.66	0.58	+13.7
1747 MHz_{1g}	0.91	0.98	0.80	+7.7
1747 MHz_{10g}	0.57	0.61	0.35	+7.0

Table 6. The 1 g and 10 g averaged SAR values for the left application side *Tilted* position for the SAM and human-head phantoms.

Type	SAR_M [W/kg]	SAR_S [W/kg]	SAR_H [W/kg]	Diff $[M-S]$ [%]
902 MHz_{1g}	0.40	0.43	0.4	+7.5
902 MHz_{10g}	0.29	0.31	0.36	+6.9
1747 MHz_{1g}	1.10	1.08	0.73	-1.8
1747 MHz_{10g}	0.66	0.65	0.32	-1.5

6.6 Performance at the SAM Head

As done in compliance testing of mobile phones, the device was placed beside the SAM standard phantom defined in [27] and originated from [35]. Figure 14 depicts the measurement setup, with the T250 phone positioned at the SAM head, as well as its corresponding CAD model within the simulation platform. The dielectric parameters of the tissue-simulating liquid were the same as previously used in Section 6.5. SAR distributions and averaged spatial peak SAR were assessed and compared for the left application side *touch* and 15° *tilted* standard test positions, as described in [2] and [27]. After importing the SAM CAD head model, the *SEMCAD* environment allowed the performance of the standard

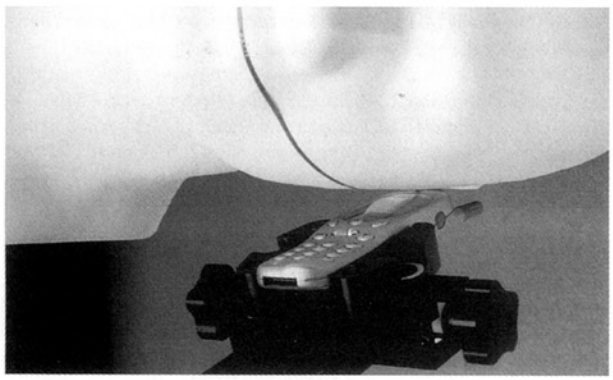

Figure 14a. The T250 phone model placed beside the SAM phantom for the measurements.

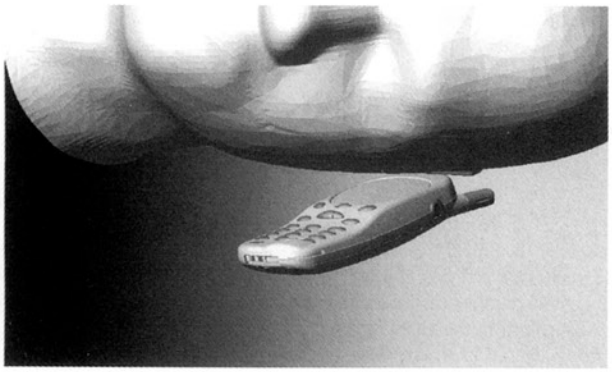

Figure 14b. The T250 phone model within the simulation platform.

Table 7. The memory and runtime requirements for the phone in free space and beside the SAM phantom setup.

Type	Base-Cells	Memory	Time
Sub $1:2_{free}$	4.5×10^6	400 MB	8 h
Graded $_{free}$	11×10^6	850 MB	≈ 30 h
Homog $_{free}$	2×10^9	≈ 150 GB	≈ 200 days
Sub $2\times1:2_{head}$	6×10^6	1 GB	14 h
Graded $_{head}$	35×10^6	2.7 GB	≈ 4 days
Homog $_{head}$	8.5×10^9	≈ 1.5 TB	≈ 2.5 years

compliance positioning using translations and rotations applied to the head phantom.

Figure 15 depicts the measured and simulated SAR distributions in the SAM phantom at a distance of 4.7 mm normal to the inner shape of the shell. The scan was performed for the left side *touch* position at $f = 1747$ MHz and was logarithmically scaled, i.e., 0 dB is equal to the maximum peak SAR value obtained in the experimental data. Good agreement was obtained between the measured and simulated distributions in the whole observation area.

The measured (*M*) and simulated (*S*) 1 g and 10 g averaged peak SAR in the left application side *touch* and 15° *tilted* positions at both frequencies are summarized in Tables 5 and 6. Good to excellent agreement between the experimental and numerical data was obtained for all configurations. The low order of differences between measurement and simulation ($\mathrm{Diff}[M-S]$) might again have resulted from cancellation of errors occurring in the uncertainties of the simulation and the tolerances of the measurement system. In the *touch* position, the SAR values showed a little dependence on the frequency. The strong variations in the 15° *tilted* position revealed the dominant influence of the high currents close to the antenna.

6.7 Performance at Human Head

In order to evaluate the performance of the phone on a human-head phantom, the device was also simulated next to the numerical model of an non-homogeneous human head (HR-EF-1) [16]. The CAD model that was imported into the *SEMCAD* platform consisted of 121 different slices (Figure 16), with slice thicknesses of 1 mm (ear region) and 3 mm and a transverse spatial resolution of 0.2 mm. Fifteen different tissue types were distinguished, the electrical parameters of which at the mobile phone frequencies were taken from [36].

The 1 g and 10 g averaged peak SAR values obtained for the HR-EF-1 head model in the *touch* and 15° *tilted* positions are presented in Tables 5 and 6 (SAR_H), in addition to the simulated (SAR_S) and measured (SAR_M) values for the SAM-phone configuration.

6.8 SAM Phantom Radiation Pattern

The three-dimensional far-field patterns of the mobile phone placed in the touch position with the SAM phantom at the GSM900 and the DCS1800 frequencies are shown in Figure 11.

6.9 Computational Requirements

The computational requirements of the simulations, including sub-grid regions, are compared to those of a simple graded-mesh approach and to those of homogeneous grids in Table 7. All computations were performed on a 1.7 GHz Intel P4 machine, operating under *LINUX*. A noticeable reduction of memory and runtime requirements was achieved for the free-space example consisting of a small simulation space. However, the comparison for larger spatial extensions, including head models, clearly revealed the need for FDTD local-refinement schemes for complex real-world configurations.

7. Conclusions

This study demonstrates that FDTD is a suitable technique for supporting engineers in the analysis, design, and optimization of transmitters, even for the most complex cases such as mobile phones operating in the vicinity of the human body. The study also clearly revealed that flexible user interfaces, as well as graded meshes combined with local-refinement schemes, are required in order to achieve the needed resolution of small details in the range

of 100 μm within locally restricted areas of a computational domain extended to one meter or more. Obvious items on the wish list for designers are shorter turnaround times and semi-automated optimization support, which are on our current research agenda, together with features for uncertainty assessments.

8. Acknowledgements

This study was supported by the Swiss Commission for Technology and Innovation (CTI); Schmid & Partner Engineering AG (SPEAG), Switzerland; Nortel, Great Britain; and the Mobile Manufacturers Forum (MMF), Belgium.

9. References

1. FCC, "Evaluating Compliance with FCC Guidelines for Human Exposure to Radio Frequency Electromagnetic Fields," Tech. Rep. Supplement C to OET Bulletin 65, Federal Communications Commission, Washington, DC, June 2001.

2. CENELEC, *EN 50360, Product Standard to Demonstrate the Compliance of Mobile Telephones with the Basic Restrictions Related to Human Exposure to Electromagnetic Fields (300 MHz-3GHz)*, Brussels, July 2001.

3. CENELEC, *EN 50361, Basic Standard for the Measurement of Specific Absorption Rate Related to Human Exposure to Electromagnetic Fields from Mobile Phones*, Brussels, July 2001.

4. IEC, IEC 106/61/CDV // prEN 62209-1:2003, "Procedure to Measure the Specific Absorption Rate (SAR) in the Frequency Range of 300 MHz to 3 GHz. Part 1: Hand-Held Mobile Wireless Communication Devices," 2003.

5. Å. Taflove, *Computational Electrodynamics – The Finite Difference Time Domain Method*, Norwood, MA, Artech House, 1995.

6. D. M. Sullivan, *Electromagnetic Simulation Using The FDTD Method*, Piscataway, NJ, IEEE Press, 2000.

7. K. S. Kunz and R. J. Luebbers, *The Finite Difference Time Domain Method for Electromagnetics*, Boca Raton, FL, CRC Press, 1993.

8. K. S. Yee, "Numerical Solution of Initial Boundary Value Problems Involving Maxwell's Equations in Isotropic Media," *IEEE Transactions on Antennas and Propagation*, **AP-14**, 1966, pp. 302-307.

9. M. A. Jensen and Y. Rahmat-Samii, "EM Interaction of Handset Antennas and a Human in Personal Communications," *Proceedings of the IEEE*, **83**, 1, January 1995, pp. 7-17.

10. M. Okoniewski and M. A. Stuchly, "A Study of the Handset Antenna and Human Body Interaction," *IEEE Transactions on Microwave Theory and Techniques*, **MTT-44**, 10, October 1996, pp. 1855-1864.

11. V. Hombach, K. Meier, M. Burkhard, E. Kühn, and N. Kuster, "The Dependence of EM Energy Absorption upon Human Head Modeling at 900 MHz," *IEEE Transactions on Microwave Theory and Techniques*, **MTT-44**, 10, October 1996, pp. 1865-1873.

12. M. A. Jensen and Y. Rahmat-Samii, "Performance Analysis of Antennas for Hand-Held Transceivers Using FDTD," *IEEE Transactions on Antennas and Propagation*, **AP-42**, 8, August 1994, pp. 1106-1113.

13. M. Burkhardt, N. Chavannes, K. Poković, T. Schmid, and N. Kuster, "Study on the FDTD Performance for Transmitters in Complex Environments," *Proceedings of the ICECOM*, Dubrovnik, October 1997, pp. 83-86.

14. J. S. Colburn and Y. Rahmat-Samii, "Human Proximity Effects on Circular Polarized Handset Antennas in Personal Satellite Communications," *IEEE Transactions on Antennas and Propagation*, **AP-46**, 6, June 1998, pp. 813-820.

15. R. Holland, "Pitfalls of Staircase Meshing," *IEEE Transactions on Electromagnetic Compatibility*, **EMC-35**, 4, November 1993, pp. 434-439.

16. M. Burkhardt, *Contributions toward Uncertainty Assessments and Error Minimization of FDTD Simulations Involving Complex Dielectric Bodies*, PhD Dissertation, Diss. ETH Nr.13176, Zurich, 1999.

17. K. S. Nikita, M. Cavagnaro, P. Bernardi, N. K. Uzunoglu, S. Pisa, E. Piuzzi, J. N. Sahalos, G. I. Krikelas, J. A. Vaul, P. S. Excell, G. Cerri, S. Chiarandini, R. DeLeo, and P. Russo, "A Study of Uncertainties in Modeling Antenna Performance and Power Absorption in the Head of a Cellular Phone User," *IEEE Transactions on Microwave Theory and Techniques*, **MTT-48**, 12, December 2000, pp. 2676-2685.

18. A. D. Tinniswood, C. M. Furse, and O. P. Gandhi, "Computations of SAR Distributions for Two Anatomically Based Models of the Human Head Using CAD Files of Commercial Telephones and the Parallelized FDTD Code," *IEEE Transactions on Antennas and Propagation*, **AP-46**, 6, June 1998, pp. 829-833.

19. A. Schavioni, P. Bertotto, G. Richiardi, and P. Bielli, "SAR Generated by Commercial Cellular Phones – Phone Modeling, Head Modeling and Measurements," *IEEE Transactions on Microwave Theory and Techniques*, **MTT-48**, 11, November 2000, pp. 2064-2071.

20. O. P. Gandhi, G. Lazzi, A. Tinniswood, and Q.-S. Yu, "Comparison of Numerical and Experimental Methods for Determination of SAR and Radiation Patterns of Handheld Wireless Telephones," *Bioelectromagnetics*, **20**, 1999, pp. 93-101.

21. M. Jayawardene, O. Leisten, P. McEvoy, R. Seager, J. C. Vardaxoglou, and A. Wingfield, "Comparative Study of Numerical Simulation Packages for Analysing Miniature Dielectric-Loaded Bifilar Antennas for Mobile Communication," *Eleventh International Conference on Antennas and Propagation*, IEE, London, UK, **1**, 2001, pp. 260-264.

22. M. Siegbahn, "Master Thesis: A Mesh Refinement Method for FDTD and Calculations on Helical Antennas for Mobile Communications," Tech. Rep., Uppsala University School of Engineering, Sweden, 1996.

23. W. Heinrich, K. Beilenhoff, P. Mezzanotte, and L. Roselli, "Optimum Mesh Grading for Finite-Difference Method," *IEEE*

Transactions on Microwave Theory and Techniques, **MTT-44**, 9, September 1996, pp. 1569-1574.

24. SEMCAD, "Reference Manual for the SEMCAD Simulation Platform for Electromagnetic Compatibility, Antenna Design and Dosimetry," SPEAG - Schmid & Partner Engineering AG (see http://www.semcad.com).

25. N. Chavannes and N. Kuster, "Advantages and Limitations of FDTD Subgrid Schemes for EM Transmitters Embedded within Highly Complex Environments," *Proceedings of the 16th International Conference on Applied Electromagnetics and Communications ICECOM*, Dubrovnik, Croatia, October 2001, pp. 85-89.

26. T. Schmid, O. Egger, and N. Kuster, "Automated E-Field Scanning System for Dosimetric Assessments," *IEEE Transactions on Microwave Theory and Techniques*, **MTT-44**, January 1996, pp. 105-113.

27. IEEE, Std. 1528, *Recommended Practice for Determining the Peak Spatial-Average Specific Absorption Rate (SAR) in the Human Head from Wireless Communications Devices: Measurement Techniques*, Final Draft, November 2003.

28. K. Meier, M. Burkhardt, T. Schmid, and N. Kuster, "Broadband Calibration of E-Field Probes in Lossy Media," *IEEE Transactions on Microwave Theory and Techniques*, **MTT-44**, 10, October 1996, pp. 1954-1962.

29. Katja Poković, Thomas Schmid, and Niels Kuster, "Robust Setup for Precise Calibration of E-Field Probes in Tissue Simulating Liquids at Mobile Communications Frequencies," ICECOM'97, Dubrovnik, October 15-17, 1997, pp. 120-124.

30. M. J. Piket-May, A. Taflove, and J. Baron, "FD-TD Modeling of Digital Signal Propagation in 3-D Circuits with Passive and Active Loads," *IEEE Transactions on Microwave Theory and Techniques*, **MTT-42**, 1994, pp. 1514-1523.

31. J. P. Berenger, "A Perfectly Matched Layer for the Absorption of Electromagnetic Waves," *Journal of Computational Physics*, October 1994.

32. A. Taflove and K. R. Umashankar, "Radar Cross Section of General Three-Dimensional Structures," *IEEE Transactions on Electromagnetic Compatibility*, **EMC-25**, 1983, pp. 433-440.

33. A. Drossos, V. Santomaa, and N. Kuster, "The Dependence of Electromagnetic Energy Absorption upon Human Head Tissue Composition in the Frequency Range of 300-3000 MHz," *IEEE Transactions on Microwave Theory and Techniques*, **MTT-48**, 11, November 2000, pp. 1988-1995.

34. Subcommittee 2 IEEE SCC-34, *P1529/2000X, Recommended Practice for Determining the Spatial-Peak Specific Absorption Rate (SAR) Associated with the Use of Wireless Handsets – Computational Techniques*, Piscataway, NJ, September 2000.

35. Gordon et al., *Anthropomorphic Survey of U.S. Army Personnel: Methods and Summary Statistics*, Technical Report NATICK/TR-89/044, 1989.

36. C. Gabriel, "Compilation of the Dielectric Properties of Body Tissues at RF and Microwave Frequencies," Tech. Rep., Report N.AL/OE-TR-1996-0037, Occupational and Environmental Health Directorate, Radiofrequency Radiation Division, Brooks Air Force Base, Texas (USA), June 1996.

Introducing the Feature Article Authors

Nicolas Chavannes was born in Bern, Switzerland, in April, 1972. He received the MS and PhD degrees in Electrical Engineering from the Swiss Federal Institute of Technology (ETH), Zurich, in 1998 and 2002, respectively. In 1996, he joined the Bioelectromagnetics/EMC Group (BIOEM/EMC) at ETH Zurich, where he was involved in computational electrodynamics and related dosimetric applications. From 1998 to 2002, he was with the Laboratory for Electromagnetic Fields and Microwave Electronics (IFH) as well as the Laboratory for Integrated Systems (IIS), both located at ETH Zurich. His research activities there were focused on the development of FDTD local refinement techniques and their application to numerical near-field analysis. In late 1999, he joined the Foundation for Research on Information Technologies in Society (IT'IS), Switzerland, where he is currently in charge of the development and extension of a simulation platform targeted for antenna modeling and mobile telecommunications equipment design in complex environments, dosimetry, and optics applications. In early 2002, he joined Schmid & Partner Engineering AG (SPEAG), Zurich, Switzerland, as head of the software R&D team. His primary research interests include the development, implementation, and application of computational modeling and simulation techniques to electromagnetics in general, and to antennas as well as bioelectromagnetic interaction mechanisms, in particular.

Roger Yew-Siow Tay received the BS and the MS degrees in Electrical Engineering from the University of Massachusetts, Lowell, in 1983 and 1985, respectively, and the PhD degree from the Swiss Federal Institute of Technology (ETH), Zurich, Switzerland, in 1997. He is currently a Distinguished Member of the Technical Staff at Motorola's Global Center of Excellence in Singapore. He leads the Advance Electrical Engineering team in the design and development of cellular phones. He set up the Electromagnetics Laboratory in the Motorola Singapore facility, and installed the first SAR measurement system based on the DASY system in Southeast Asia. His interests include antennas for personal communication devices, antenna metrology, dosimetry, and techniques to modularize transceiver system for wireless communication devices. He holds eight US patents and several pending patents, and has contributed papers to many journals and confer-

ences. Dr. Tay is a member of the IEEE Antennas and Propagation, Vehicular Technology, Communications, and Electromagnetic Compatibility Societies. He is also a Committee Member of the Singapore Chapter of the IEEE EMC Society.

Neviana Nikoloski was born in Bulgaria in November, 1972. She received her MS in Engineering Physics from Sofia University "St. Kliment Ohridsky," Bulgaria, in 1996, and is currently working toward her PhD degree at the Swiss Federal Institute of Technology (ETH), Zurich, Switzerland. In 2000, she joined the Foundation for Research on Information Technologies in Society (IT'IS), Zurich, where she is involved in dosimetric evaluations, as well as the design and optimization of in-vivo and in-vitro RF exposure setups for risk assessment of EMF exposure by mobile phones. N. Nikoloski is a student member of the Bioelectromagnetics Society (BEMS). She received the first and second place BEMS Curtis Carl Johnson Memorial Awards in 2003 and 2002, respectively.

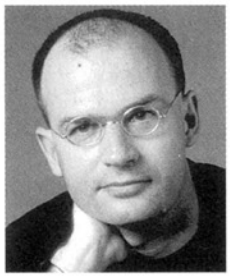

Niels Kuster was born in 1957 in Olten, Switzerland. He received the MS and PhD degrees in Electrical Engineering from the Swiss Federal Institute of Technology (ETH) in Zurich. In 1993, he was elected Professor at the Department of Electrical Engineering of the Swiss Federal Institute of Technology (ETH) in Zurich, Switzerland. In 1992, he was an Invited Professor at the Electromagnetics Laboratory of Motorola, Inc., in Florida, USA, and in 1998 at the Metropolitan University of Tokyo, Japan. In 1999, he was appointed Director of the Foundation for Research on Information Technologies in Society, Switzerland. His research interests are currently focused on the area of reliable on/in-body wireless communications and related topics. This includes measurement technology; computational electrodynamics for evaluation of close near fields in complex environments; safe and reliable wireless-communication links within the body or between implanted devices and the outside for biometrics applications; development of exposure setups and quality control for biological experiments evaluating interaction mechanisms and therapeutic effects as well as potential health risks; and exposure assessments.